Predicting toxic potencies of metal oxide nanoparticles by means of nano-QSARs

Yunsong Mu, Fengchang Wu, Qing Zhao, Rong Ji, Yu Qie, Yue Zhou, Yan Hu, Chengfang Pang, Danail Hristozov, John P. Giesy & Baoshan Xing

View supplementary material ⚹

Accepted author version posted online: 16 Jun 2016.
Published online: 11 Jul 2016.

Submit your article to this journal ⚹

Article views: 75

View related articles ⚹

View Crossmark data ⚹

SHORT COMMUNICATION

Predicting toxic potencies of metal oxide nanoparticles by means of nano-QSARs

Yunsong Mu[1], Fengchang Wu[1], Qing Zhao[2], Rong Ji[3], Yu Qie[1], Yue Zhou[3], Yan Hu[1], Chengfang Pang[4], Danail Hristozov[4], John P. Giesy[5], and Baoshan Xing[6]

[1]State Key Laboratory of Environmental Criteria and Risk Assessment, Chinese Research Academy of Environmental Sciences, Beijing, China, [2]Institute of Applied Ecology, Chinese Academy of Sciences, Shenyang, China, [3]State Key Laboratory of Pollution Control and Resource Reuse, School of the Environment, Nanjing University, Nanjing, China, [4]Department of Environmental Sciences, Informatics and Statistics, University Ca' Foscari of Venice, Venice, Italy, [5]Toxicology Centre, University of Saskatchewan, Saskatoon, Canada, and [6]Stockbridge School of Agriculture, University of Massachusetts, Amherst, USA

Abstract

Background: The enormous physicochemical and structural diversity of metal oxide nanoparticles (MeONPs) poses significant challenges to the testing of their biological uptake, biodistribution, and effects that can be used to develop understanding of key nano-bio modes of action. This has generated considerable uncertainties in the assessment of their human health and environmental risks and has raised concerns about the adequacy of their regulation. In order to surpass the extremely resource intensive case-by-case testing, intelligent strategies combining testing methods and non-testing predictive modeling should be developed.
Methods: The quantitative structure-activity relationship (QSARs) in silico tools can be instrumental in understanding properties that affect the potencies of MeONPs and in predicting toxic responses and thresholds of effects.
Results: The present study proposes a predictive nano-QSAR model for predicting the cytotoxicity of MeONPs. The model was applied to test the relationships between 26 physicochemical properties of 51 MeONPs and their cytotoxic effects in Escherichia coli. The two parameters, enthalpy of formation of a gaseous cation ($\triangle H_{me+}$) and polarization force (Z/r), were elucidated to make a significant contribution for the toxic effect of these MeONPs. The study also proposed the mechanisms of toxic potency in *E. coli* through the model, which indicated that the MeONPs as well as their released metal ions could collectively induce DNA damage and cell apoptosis.
Significance: These findings may provide an alternative method for prioritizing current and future MeONPs for potential in vivo testing, virtual prescreening and for designing environmentally benign nanomaterials.

Introduction

Metal oxide nanoparticles (MeONPs) have been widely used across various sectors including information and communication technologies, healthcare, transportation and construction. Among all currently produced materials that explicitly claim nanoscale properties, 80% are metals or metal oxides with annual production of approximately 242 000 tonnes, of which $>95\%$ are TiO_2, ZnO, Al_2O_3, Fe_2O_3, and SiO_2 (Markets, 2015). They offer an array of promising applications as constituents of sunscreens, cosmetics, textiles, medical products and electronic devices (De et al., 2008). However, significant data gaps and uncertainties have prevented their robust human health and environmental risk assessment (Lubick, 2008), which has raised concerns about the adequacy of their regulation. The underlying issue is the enormous complexity caused by the physicochemical and structural diversity of

MeONPs, which poses significant challenges to the testing of their biological uptake, bio-distribution, and effects in order to develop understanding of key nano-bio interactions and relevant toxicological modes of action. The data gaps and uncertainties can be reduced through extensive *in vivo* testing complemented by robust physicochemical characterization. Therefore, there are growing concerns that their unique nanoscale properties (e.g. surface characteristics, interface and quantum size) might induce specific biological effects, pose a threat to ecosystem and human health (Yin et al., 2013). Some nanoscale metal oxides (e.g. CuO, ZnO and TiO_2) might be more toxic than that of carbon nanoparticles and multi-walled carbon nanotubes (Karlsson et al., 2008). They can produce reactive oxygen species (ROS) (Wilson et al., 2002) as well as modulation of inflammatory responses, which play important roles in their toxicities at the organism and cellular levels (Brown et al., 2001).

Given the enormous diversity and multitude of MeONPs reaching the market, this effort would be extremely resource-intensive and in conflict with the principle for replacement, reduction, and refinement of animal testing. Therefore, it is essential to establish efficient testing strategies for the MeONPs

Correspondence: Fengchang Wu, State Key Laboratory of Environmental Criteria and Risk Assessment, Chinese Research Academy of Environmental Sciences, Beijing 100012, China. Tel: +86–1084915312. Fax: +86–1084931804. E-mail: wufengchang@vip.skleg.cn

that combine *in vivo* experiments with *in vitro* models and computational *in silico* modeling methods. While there have been some fundamental researches on toxic effects of nanomaterials (Nel et al., 2015; Sarkar et al., 2014), it was important to develop a conceptual framework that could be used to predict toxic potencies and identify toxic mechanisms before their use in various applications.

For a series of substances with the same mode of action, quantitative structure-activity relationships (QSARs) can statistically correlate physicochemical and structural properties of MeONPs with their biological activity. Thus, QSAR or similar *in silico* predictive tools can be useful as theoretical constructs to facilitate better understanding of certain mechanisms of toxicity in order to enable grouping and ''read-across'' strategies (Chen et al., 2015; Mu et al., 2014; Wu et al., 2010, 2013). Such strategies are needed as the multitude and variety of the MeONPs reaching the market make their case-by-case risk assessment very expensive both in terms of testing costs and sacrificed experimental animals (Winkler et al., 2013). This has turned nano-QSAR into a dynamic area of research, where more than 20 physicochemical properties have been identified as predictive of the toxicity of MeONPs. While a minimal set of physicochemical parameters that should be considered in the development of nano-QSARs is still under discussions (Pathakoti et al., 2014; Schrurs & Lison, 2012), much remains to be learned about the relationships between nanoscale properties and biological outcomes. (Meng et al., 2009; Zhao et al., 2014). Some predictive models of nanoparticles uptake by cells and apoptosis were developed and a strategy for modeling was applied for various nanoparticles or modifications of their surfaces. (Epa et al., 2012; Pang et al., 2016; Zhang et al., 2012). A model to describe toxic potencies of 17 MeONPs in *Escherichia coli* based on enthalpy of formation of gaseous ions was recently proposed. (Puzyn et al., 2011). However, this model needs to be further developed in order to obtain better predictive capacity for determination of toxicological mode of action.

In the present study, the relationships between 26 physico-chemical properties and the cytotoxicity of MeONPs in *E. coli* were examined using multiple linear regressions (MLR). The optimal structure parameters of 16 MeONPs were developed, describing the properties of both MeONPs and metal ions released from them. In addition, cytotoxicities of 51 MeONPs, except for the alkali metal oxides and most alkaline-earth metal oxides in the periodic table, were predicted by means of a feasible nano-QSAR model, for which no empirical toxicity data were available and especially for those that had not yet been synthesized or had not yet been used on an industrial scale. To show the feasibility of constructing nano-QSARs, two commercially available MeONPs were tested in concentrations needed to yield EC_{50} value. Therefore, it is not mainly concerned on the relation to environmentally realistic concentration in the context. The proposed nano-QSAR model provided some advantages over previous methods, making an improvement in calculation of structural parameters, development of predictive capacity, and explanation for mode of action. This *in silico* modeling approach proved to be an effective solution to overcome current scarcity of toxicity data for a variety of MeONPs and to guide the design of safer nanomaterials.

Methods

Biological data and nanoscale structural properties

Data on the toxic potencies of 16 MeONPs to *E. coli* were obtained from the literature and laboratory experiments that were expressed in terms of the negative logarithm of EC_{50} (mol/L) (Hu et al., 2009; Puzyn et al., 2011). Twenty-six physicochemical properties of 51 MeONPs were calculated (1326 data points), which contained physicochemical, scale, and thermodynamic properties of both nanoparticles and metal ions (Table 1). Three-dimensional structures were prepared using the previously described methods (Puzyn et al., 2011). Calculations were made at the semi-empirical theoretical level using PM6 methods in the

Table 1. Clustering, principal component analysis and evaluating contributions of each parameter.

| Properties | Descriptions | Principle components | | | |
		1 43.170	2 71.583	3 84.537	4 90.137
ΔH_{me+}	Enthalpy of formation of a gaseous cation	0.812	0.524	−0.088	0.139
σp	Softness index	−0.235	−0.681	0.455	0.248
$\sigma p/Z$	Softness index per ion charge	−0.755	−0.597	−0.019	−0.047
AN	Atomic number	−0.292	0.780	0.479	0.252
r	Pauling ionic radius	−0.479	0.429	0.722	0.151
ΔIP	Difference in $IP(N+1)$ and IP	0.678	−0.390	0.153	0.408
ΔE_0	Electrochemical potential	0.352	−0.569	0.601	0.162
X_m	Electro negativity	−0.492	0.579	−0.566	0.194
$|logK_{OH}|$	First hydrolysis constants	−0.652	−0.556	−0.127	−0.187
$X_m{}^2r$	Covalent index	−0.605	0.722	−0.043	0.275
Z^2/r	Polarization force parameters	0.962	0.231	−0.029	−0.037
$AN/\Delta IP$	Atomic ionization potential	−0.626	0.703	0.159	0.227
AR	Atomic radius	−0.030	−0.643	−0.066	0.549
IP	IP values for the O_N state of the ion	0.888	0.420	−0.110	−0.053
$IP(N+1)$	IP values for the $O_{(N+1)}$ state of the ion	0.845	−0.189	0.091	0.321
AW	Atomic weight	−0.273	0.779	0.483	0.262
AR/AW	Electron density	0.311	−0.722	−0.404	0.329
Z	Ionic charge	0.869	0.407	0.240	0.047
Z/r^2	Polarization force parameters	0.893	−0.094	−0.401	0.061
Z/AR^2	Similar polarization force parameters	0.643	0.629	0.164	−0.290
Z/r	Polarization force parameters	0.968	0.088	−0.206	0.021
Z/AR	Similar polarization force parameters	0.760	0.570	0.205	−0.163
x	Electro negativity	−0.495	0.576	−0.567	0.193
Z/rx	Relative softness	0.974	−0.138	0.096	−0.043
GAP	Energy difference between HOMO and LUMO energies	−0.384	−0.226	0.490	−0.389
HoF	Standard heat of formation of the oxide cluster	−0.439	0.501	−0.575	0.034

MOPAC 2012 software package (Colorado Springs, CO, USA) (Tamura, 2010). The descriptors could reliably reflect various properties of MeONPs, which included enthalpy of formation of a gaseous cation (ΔH_{me+}), energy difference between HOMO and LUMO energies (GAP), and standard heat of formation (HoF) (Puzyn et al., 2011). Twenty-three properties of metal ions released from the MeONPs included: softness index (σp), ionic charge (Z), softness index per ion charge ($\sigma p/Z$) (Pearson & Mawby, 1967); atomic number (AN), difference in ionization potentials between the $O_{(N+1)}$ state ($IP(N+1)$) and O_N state (IP) of the ion (ΔIP), and atomic ionization potential ($AN/\Delta IP$) (Kaiser, 1980; Mccloskey et al., 1996; Wolterbeek & Verburg, 2001); electro negativity (X_m), Pauling ionic radius (r), and covalent index ($X_m^2 r$) (Wolterbeek & Verburg, 2001); electro-chemical potential (ΔE_0) (Kaiser, 1980); first hydrolysis constants ($|\log K_{OH}|$) (Base & Mesmer, 1976); relative softness (Z/rx) where x represents electro-negativity values, atomic radius (AR), atomic weight (AW), and electron density (AR/AW) (Wolterbeek & Verburg, 2001); polarization force parameters (Z/r, Z/r^2 and Z^2/r), and similar polarization force parameters (Z/AR and Z/AR^2) (Mccloskey et al., 1996).

The above descriptors are size-independent, which seems to be in conflict with the widely accepted notion that the size of MeONPs is decisive for their toxicity. However, the reason is that a preliminary investigation on nanoparticles of different sizes have revealed that some molecular descriptors (e.g. ΔH_{me+} and HoF) correlate linearly with the cluster size (Gajewicz et al., 2011). Moreover, the size-dependent change of some electronic properties (e.g., ΔIP and X_m) occurs below about 5 nm (Zhai & Wang, 2007). The variation of property with the increasing size of the nanomaterials does not occur until it reaches the saturation point. Therefore, we assumed that the clusters must be of the same size and bigger than 5 nm for all the studied oxides.

Modeling

We use MLR, combined with Pearson and pair-wise correlations, clustering and principal component analysis to obtain optimal structure descriptors, to build a simple linear QSAR model that provided a quick estimate of the cytotoxicity to *E. coli*. The Pearson correlation coefficients (R^2) between pairs of structural parameters were calculated to avoid auto-correlation, and then used to select parameters maintained in models. Clustering and principal component analyses (PCA) were performed on the structure properties that had significant correlations with observed toxicities ($R > 0.8$). Combinations of four parameters, Z/r, IP, ΔH_{me+} and $\sigma p/Z$, were used as independent variables, since they made excellent contributions to the first principle component. The coefficient of determination (r^2) and the root mean square error (RMSE) were applied as measures of the goodness-of-fit. Obtained data were statistically analyzed using analysis of variance (ANOVA) and expressed as the mean with standard error. The obtained F-value was compared with the corresponding critical value ($p = 0.05$). A value of $p < 0.05$ was considered statistically significant. Calculations were made with the QSAR toolbox in the SYBYL X1.1 program (Tripos, Inc. Co, Princeton, NJ, USA) and SPSS statistics 17.0 (IBM, Chicago, IL, USA).

Internal validation and statistical measures of robustness

Internal validation was conducted to assess predictive ability, sensitivity and reliability of the models and chance correlation was assessed by three methods, including leave-one-out (LOO), leave-many-out (LMO, $m = 3$), and bootstrapping (Golbraikh et al., 2003; Tropsha et al., 2003). To avoid autocorrelations and to confirm the robustness of the QSAR model, progressive

scrambling analyses (randomization: 50, maximum: five bins, minimum: two bins and critical point: 0.75) were also performed. In the progressive randomization approach, small random perturbations were introduced into the training set. The statistical results included the predicted perturbation (Q^2), the calculated cross-validated standard error of prediction (SEP_{CV}) expressed as a function of the correlation coefficient between the true values (y) and the perturbed values (y') of the dependent variables, and the slope of Q^2 with respect to the correlation of the original-dependent variables against the perturbed-dependent variables (dq^2/dr^2_{yy}) (Clark & Fox, 2004). The QSAR models that change greatly with small changes in underlying responses are unstable, which are characterized by slopes greater than 1.20.

Empirical toxicity testing

The two types of the nanoparticles that were tested empirically, Mn_2O_3 (99.2%, TEM, 30 nm) and Co_3O_4 (99%, TEM, 10–30 nm), were purchased from US Research Nanomaterials, Inc (Houston, TX, USA). The *E. coli* (wild type) was cultured at $37\,^\circ$C overnight using Luria-Bertani (LB) broth. Cultures were centrifuged at $3000\,g$ for 10 min and resuspended in sterilized physiological saline. Densities of cultures of bacteria were adjusted to 0.5×10^9–1.66×10^9 cells/mL as determined by enumeration of colony forming units on LB Petri dishes.

Cytotoxicities of nanoparticles were expressed in terms of the negative logarithm of EC_{50}, which is the effective concentration of a given oxide that reduces viability of cells of bacteria by 50%. Heterotrophic mineralization of glucose by bacteria was also identified as a measure of the rate of metabolism of the selected samples. After being washed three times with physiological saline, 0.1 mL suspensions of *E. coli* were added to 2 mL of distilled water (control) or 2 mL of nanoparticles/distilled water solution at the nominal concentrations of 200, 400, and 600 mg/L, respectively. To ensure dispersal of nanoparticles, stock solutions were prepared at a concentration of 1.2 g/L after sonication (Fisher Scientific FS30 Ultrasonic Cleaner, Marshall Scientific, Hampton, NH, USA) at $25\,^\circ$C for 20 min. Suspensions were sonicated again for 10 min just before commencement of the exposure experiments. Both control and experimental groups were then agitated for 2 h at 150 rpm. Rates of metabolism were measured by quantification of $^{14}CO_2$ released during metabolic respiration of uniformly radioactive labeled UL-^{14}C-D-glucose (specific radioactivity 3 mCi/mmol, American Radio-labeled Chemicals, St. Louis, MO, USA) dissolved in ethanol following the 2 h incubation period.

At time zero, the 50 mL glass vial was sealed with a silicone stopper, on the bottom of which was hung a needle with a folded filter paper soaked with 0.05 mL of 4 mol/L NaOH solution for CO_2 trapping. Trapping occurred overnight (8–12 h) after injection with 1 mol/L H_2SO_4 at the end of 2 h incubation. Filter papers were then removed and placed in 6 mL scintillation vials containing 1 mL of 1 mol/L NaOH. Then 3 mL scintillation cocktail (Gold Star multi-purpose, Maridian Biotechnology Ltd, Epsom, UK) was added to the scintillation vials and radioactivity was quantified by counting with a liquid scintillation counter (LS-6500, Beckman-Coulter, Series Liquid Scintillation Counters, Brea, CA, USA). Concentrations were calculated from disintegrations per minute (DPM) and the specific activity of the mixture.

External validation and applicability domain of the model

To ensure that there was no systematic error due to variation under laboratory conditions, measurements of toxicity among a series of experiments were repeated for Mn_2O_3 and Co_3O_4. These two commercially available MeONPs were tested for external

validation. Measures of predictive ability based on external validation can be expressed as the root mean square error of prediction (*RMSEP*) (Equation 1).

$$RMSEP = \sqrt{\frac{\sum_{i=1}^{v}(y_i^{obs} - y_i^{pred})^2}{v}} \quad (1)$$

where: y_i^{obs} is experimental (observed) value of the property for the *i*th compound; y_i^{pred} is predicted value for *i*th compound; *v* is the number of compounds in the validation set.

Responses were also verified by the use of response and structure space of MeONPs, in which the model makes predictions with the most optimal reliability. In the present study, the leverage approach and Williams plots were used to visualize results (Tropsha et al., 2003). Defining borders of the space, which is referred to as the ''optimum prediction space' or 'applicability domain', is important, especially for compounds with unavailable experimental data to verify quality of predictions. If the standardized residual of a compound is greater than three standard deviation units ($\pm 3\sigma$), the compound is classified as an outlier that might be less reliable and thus treated with greater care (Dearden et al., 2009). The leverage value h_i for each ith compound is calculated from the descriptor matrix (*X*) (Equation 2).

$$h_i = x_i^{T}(X^{T}X)^{-1}x_i \quad (2)$$

where: x_i is a row vector of molecular descriptors for a particular compound. The value of h_i greater than the warning *h** value indicates that the structure of a compound substantially differs from those used for the calibration. Therefore, the compound is located outside the optimum prediction space. The *h** value is defined (Equation 3).

$$h^* = \frac{3(p+1)}{n} \quad (3)$$

where: *p* is the number of variables used in the model and *n* is the number of training compounds.

Results

Quantitative nanostructure-activity relationship studies on MeONPs

QSAR models for 16 MeONPs were developed and then used to predict cytotoxicities of 35 nanoparticles for which data on toxicity to *E. coli* were not available (Puzyn et al., 2011). Although the number of nanoparticles was limited, it was enough to build a predictive model. Twenty-six structure descriptors were obtained by employing semi-empirical quantum chemistry calculations or from informations in the literature. These descriptors represent physicochemical properties at the molecular scale, properties of surface and valence, physicochemical properties of free metal ions, describing dissolution and ionization potentials of metal ions released from MeONPs that were used in development of the QSAR models (Table S1, SI). After an initial assessment of associations on the basis of Pearson and pair-wise coefficients of determination (r^2) (Table S2, SI), clustering and principal component analyses (Table 1) were performed to help select four optimal parameters (e.g., Z/r, *IP*, ΔH_{me+}, and $\sigma p/Z$) and establish multiple linear regression models. After assessing some developed models, an optimal two-variable model was selected (Table 2). A simple but statistically significant QSAR model was developed to predict toxicities of nanomaterials (Equation 4). Statistical indicators of this model were as follows, $R^2 = 0.8793$, *RMSE* = 0.442, *F* = 55.654, and *p* = 4.23 $\times 10^{-7}$, which means that these two descriptors can

Table 2. Summary of model performance using different parameter sets[a].

Properties	No.	r^2	F	p	Multiple linear regression model
Z/r, *IP*, ΔH_{me+}, $\sigma p/Z$	4	0.8614	24.306	2.05×10^{-05}	$T = (4.88 \pm 0.86) + (-0.09 \pm 0.11)Z/r + (-0.01 \pm 0.02)IP + (-0.01 \pm 4.74 \times 10^{-4})\Delta H_{me+} + (-5.49 \pm 9.84)\sigma p/Z$
Z/r, *IP*, ΔH_{me+}	3	0.8693	34.270	3.65×10^{-06}	$T = (4.41 \pm 0.17) + (-0.16 \pm 0.10)Z/r + (-0.01 \pm 0.02)IP + (-0.01 \pm 3.89 \times 10^{-4})\Delta H_{me+}$
Z/r, ΔH_{me+}, $\sigma p/Z$	3	0.8717	34.961	3.28×10^{-06}	$T = (4.74 \pm 0.72) + (-0.12 \pm 0.07)Z/r + (-0.01 \pm 4.37 \times 10^{-4})\Delta H_{me+} + (-3.95 \pm 8.35)\sigma p/Z$
IP, ΔH_{me+}, $\sigma p/Z$	3	0.8657	33.216	4.31×10^{-06}	$T = (5.17 \pm 0.76) + (-0.02 \pm 0.01)IP + (-0.01 \pm 4.59 \times 10^{-4})\Delta H_{me+} + (-9.01 \pm 8.65)\sigma p/Z$
Z/r, *IP*, $\sigma p/Z$	3	0.8030	21.374	4.19×10^{-05}	$T = (3.75 \pm 0.87) + (-0.14 \pm 0.13)Z/r + (-0.03 \pm 0.03)IP + (7.48 \pm 9.90)\sigma p/Z$
Z/r, *IP*	2	0.8095	32.860	8.24×10^{-06}	$T = (4.38 \pm 0.21) + (-0.10 \pm 0.11)Z/r + (-0.05 \pm 0.02)IP$
Z/r, ΔH_{me+}	2	0.8793	55.654	4.23×10^{-07}	$T = (4.412 \pm 0.165) + (-0.121 \pm 0.068)Z/r + (-0.001 \pm 2.57 \times 10^{-4})\Delta H_{me+}$
Z/r, $\sigma p/Z$	2	0.8054	32.046	9.44×10^{-06}	$T = (3.12 \pm 0.52) + (-0.24 \pm 0.07)Z/r + (14.49 \pm 6.23)\sigma p/Z$
IP, ΔH_{me+}	2	0.8648	48.954	8.88×10^{-07}	$T = (4.40 \pm 0.18) + (-0.02 \pm 0.01)IP + (-9.93 \times 10^{-4} \pm 3.95 \times 10^{-4})\Delta H_{me+}$
IP, $\sigma p/Z$	2	0.8006	31.117	1.11×10^{-05}	$T = (4.11 \pm 0.80) + (-0.06 \pm 0.02)IP + (3.00 \pm 9.03)\sigma p/Z$
ΔH_{me+}, $\sigma p/Z$	2	0.8551	45.250	1.39×10^{-06}	$T = (4.86 \pm 0.76) + (-0.01 \pm 3.58 \times 10^{-4})\Delta H_{me+} + (-6.24 \pm 8.75)\sigma p/Z$
Z/r	1	0.7442	44.643	1.04×10^{-05}	$T = (4.22 \pm 0.23) + (-0.35 \pm 0.05)Z/r$
IP	1	0.8133	66.341	1.11×10^{-06}	$T = (4.37 \pm 0.21) + (-0.06 \pm 0.01)IP$
ΔH_{me+}	1	0.8602	93.263	1.44×10^{-07}	$T = (4.34 \pm 0.17) + (-0.001 \pm 1.49 \times 10^{-4})\Delta H_{me+}$
$\sigma p/Z$	1	0.6403	27.704	1.20×10^{-04}	$T = (1.40 \pm 0.27) + (30.72 \pm 5.84)\sigma p/Z$

[a]r^2 is coefficient of determination and *p* is the statistical significance level.
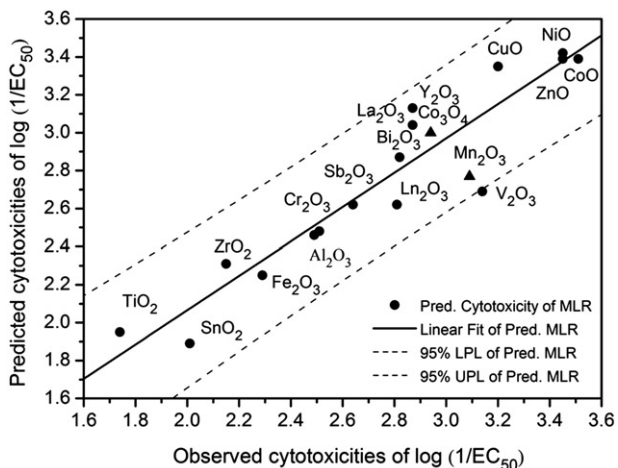
Figure 1. Observed toxic potencies as a function of predicted toxic potencies, given as $\log (1/EC_{50})$. The straight line represents perfect agreement between experimental and calculated values. Bold dots represent values predicted for the metal oxides from the training set; triangles represent the data from the external validation sets. The distance of each symbol from the line corresponds to its deviation from the related experimental value, which is within the range of 95% prediction level.

explain approximately 88% of the variability within the toxicity data.

$$\log(1/EC_{50}) = (4.412 \pm 0.165) + (-0.121 \pm 0.068)Z/r \\ + (-0.001 \pm 2.57 \times 10^{-4})\Delta H_{me+} \quad (4)$$

Validation and prediction of the nano-QSAR model

Predicted cytotoxicities of the 16 MeONPs were in a good agreement with observed ones ($R^2 = 0.882$, $F = 113.14$, $p = 0.001$) (Figure 1). Internal validation of the QSAR model was performed by use of the "leave-one-out", "leave-many-out", "bootstrapping", and "progressive scrambling" methodologies (Table S3, SI). The recommended reference criteria are $R^2 > 0.81$ and the difference between R^2 and Q_{CV}^2 does not exceed 0.3 (Eriksson et al., 2003). The progressive scrambling results indicated that the model was robust and the chance correlation did not occur with $dq^2/dr^2_{yy} < 1.20$ (Kubinyi, 1993) (Figure S1, SI). The leverage value "h" indicates the optimal applications domain of the model where the structures of tested MeONPs change (h (ΔH_{me+}) $< h^*$ and h (Z/r) $< h^*$) (Figure S2, SI). External validation, in which the toxicity testing should be consistent with the toxicities of the training sets, is also an essential part of the validation process. Toxic potency of Mn_2O_3 and Co_3O_4 had been investigated based on the effects on heterotrophic mineralization ratios of glucose by bacteria (Figure S3, SI). The predicted error between predicted and observed $\log$-EC_{50} of Mn_2O_3 was 0.37, while the predicted error of Co_3O_4 was 0.06. The predictive potency of the model was validated with a good root mean square error of prediction ($RMSEP = 0.228$).

A periodic table for cytotoxcities of MeONPs to *E. coli* was established based on the predicted model (Table S4, SI). As can be observed in the periodic table of chemical elements, there are about 80 ($\sim 65\%$) metals and 7 metalloids (e.g. B, Si, Ge, As, Sb, Se, Te and Po). From the second to the sixth period, the 51 MeONPs were in main groups of IIA-VA and subgroups of IB-VIII, with the range of predicted $\log (1/EC_{50})$ varying from 1.5 to 4.1 (Figure 2).

The proposed mechanisms of toxic potency in *E. coli*

The potential mechanisms of cytotoxicity in *E. coli* were deduced on the basis of the nano-QSAR model (Figure 3). Details of this procedure includes four steps. First, the clusters of MeONPs were accumulated through the cell membrane and interacted with proteins on the surface of the membrane. Second, the MeONPs entered into the cytoplasm through physicochemical interaction and were exposed to weakly acidic conditions, which can break the Me-O bond around the surface of the nanoparticles. Then, metal ions are involved in macromolecular complexation. In the meantime, free electrons are generated and interact with various molecules in the cell to produce reactive oxygen species (ROS). Finally, the ROS cause DNA damage and metal ions will be involved in macromolecular complexation

In the proposed mechanisms, the ΔH_{me+} characterized the capacity of the MeONPs to form free metal ions, while the Z/r characterized the capacity of free metal ions to cause toxicity. These two parameters represent the key steps in an adverse outcome pathway that resulted in toxic effects. Since diameters of the tested nanoparticles were in the range from 15 to 90 nm, the parameters used to characterize the size of the MeONPs clusters were ignored. However, in the real toxicity studies, the size of the nanomaterials also play an important role (Gliga et al., 2014). Therefore, a better model including size parameters should be developed in the future.

Discussion

The nano-QSAR model, which includes two parameters (ΔH_{me+} and Z/r), was developed from a training set of 16 individual compounds. The ratio between the number of training sets and the number of structure parameters met the criteria of Toppliss and Costello (1972). Meanwhile, the two structure parameters can contribute to characterize the mode of toxic action. The parameter ΔH_{me+}, computed from semi-empirical quantum chemistry, represents molar enthalpy of formation of gaseous ions. Release of ions from MeONPs is an important factor in induction of toxicity of MeONPs. Cations of lesser charge, are more energetically favorable than those cations with more electrons to loose. For example, nano PbO is predicted more toxic than nano PbO_2. This results are in accordance with the finding that the higher the ionic potential, the greater the degree of the ion–ion screening effects in an oxide by surrounding anions (Erdemir et al., 2005). Several studies have confirmed that the released metal ions in culture media from some nanomaterials were the proximal cause of adverse effects (Alaraby et al., 2016; Wang et al., 2014, 2016). Another parameter, Z/r, represents electro-negativity or propensity of metal ions to bind to bioligands. Inferred from the model, the binding capacity can enhance the MeONPs to cause toxic effects. Toxicities of n-ZnO and n-CuO to a bacterium (*V. fischeri*) and some crustaceans (*D. magna* and *T. platyurus*) were mostly due to dissolution of Zn^{2+} and Cu^{2+} (Heinlaan et al., 2008), which was significantly different with the toxic mechnisms of their nano-state (Lubick, 2008). Cytotoxicities of Mn_2O_3 (99.2%, TEM, 30 nm) and Co_3O_4 (99%, TEM, 10-30 nm) were tested to acquire the EC_{50} values for the purpose of external validation. These values were 192 mg/L and 245 mg/L, respectively. The values predicted by the model for these two compounds were 93 mg/L and 210 mg/L, respectively. It is important to note that these dose ranges were selected only for validation purposes and do not reflect environmentally relevant concentrations.
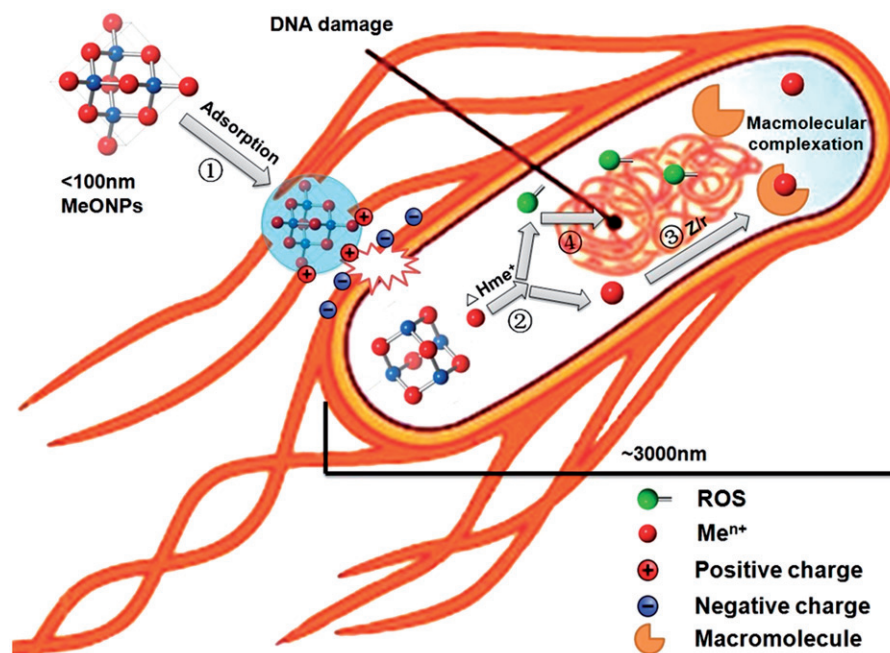
As shown in the period table, since elements in the same main group have similar extranuclear electron arrangements, toxic potencies of elements with the same valence vary with less than 1

Periodic table of predicted cytotoxicity for 51 metal oxide nanoparticles

CuO 3.35

Metal oxide nanoparticles
Predicted log (1/EC$_{50}$)

Color scale: >4, 3-4, 2-3, <2

	IIA	IIIB	IVB	VB	VIB	VIIB		VIII				IB	IIB	IIIA	IVA	VA	VIA-VIIIA
	BeO 3.22																
	MgO 3.53													Al$_2$O$_3$ 2.46			
	CaO 3.76	Sc$_2$O$_3$ 3.05	TiO$_2$ 1.95	V$_2$O$_3$ 2.69	Cr$_2$O$_3$ 2.48	Mn$_2$O$_3$/MnO$_2$ 2.77 1.9	Fe$_2$O$_3$ 2.25	CoO/Co$_3$O$_4$/Co$_2$O$_3$ 3.39 2.94 2.83	NiO 3.42	CuO 3.35	ZnO 3.39			Ga$_2$O$_3$ 2.44	GeO$_2$ 1.64		
	SrO 3.78	Y$_2$O$_3$ 3.13	ZrO$_2$ 2.31	Nb$_2$O$_3$ 2.6	Mo$_2$O$_3$ 2.58	TcO$_2$ 1.55	RuO$_2$ 1.96	Rh$_2$O$_3$ 2.91	PdO 3.22	Ag$_2$O 4.07	CdO 3.61			In$_2$O$_3$ 2.62	SnO$_2$ 1.89	Sb$_2$O$_3$ 2.62	
	BaO 3.84	La$_2$O$_3$ 3.04	HfO$_2$ 2.27	Ta$_2$O$_3$ 2.54	WO$_2$ 1.67	ReO$_2$ 1.86	OsO$_2$ 1.89	IrO$_2$ 2.23	PtO/PtO$_2$ 3.3 1.5	Au$_2$O/Au$_2$O$_3$ 4.01 2.7	HgO 3.49			Tl$_2$O/Tl$_2$O$_3$ 4.1 2.66	PbO/PbO$_2$ 3.7 1.8	Bi$_2$O$_3$ 2.87	

Figure 2. A periodic table of predicted toxic potencies of 51 MeONPs. The predicted value is described as the negative logarithm of median effect concentration, with the unit of the EC$_{50}$ defined as mol/L. The color scale of log (1/EC$_{50}$) value shows the potential assigned to each of the MeONPs, ranging for green (<2), light green (2-3), yellow (3-4), and red (>4), respectively. .

Figure 3. Proposed mechanism of toxic potency of MeONPs combined with released metal ions to *E. coli*. There are four steps as follows: (1) The MeONPs are absorbed or accumulated through the cell membrane and interacted with proteins on the surface of membrane. (2) The MeONPs enter into the cytoplasm, break the Me-O bond, and release metal ions and free electrons. (3) The metal ions are involved in macromolecular complexation. (4) The free electrons are generated and interact with various molecules in the cell to produce reactive oxygen species (ROS). Then, it attacks the DNA to cause DNA damage and cell apoptosis.

DNA damage

Adsorption

<100nm MeONPs

Macmolecular complexation

~3000nm

ROS
Me^{n+}
Positive charge
Negative charge
Macromolecule

order of magnitude. In contrast, elements in the same period have identical numbers of electrons in their outer shell, which lead to the fact that elements in IB, IIA, IIB cause adverse effects but higher valencies correlate with lower toxicity of the ions. For instance, Tl$_2$O, Ag$_2$O and Au$_2$O had the greatest toxic potency (Predicted log 1/EC$_{50}$>4), while PtO$_2$ and TcO$_2$ were less toxic (Predicted log 1/EC$_{50}$<1.6) (Table S4, SI). This result is consistent with previously reported results (Negi et al., 2013). The reason for this is that *s*-, *p*-, and *d*-metals have different oxidation states. The s-metal only has one oxidation state, but *p*-has two oxidation states. The difference between them is two units. The *d*-metal has higher valence state except for the +2 oxidation state. For example, lanthanide and actinide metals have fully occupied *d^{10}* orbitals, with significant differences among ionic radii and atomic radii. Moreover, it was also found that MeONPs, which were less oxidized, exhibited greater toxic potencies. For instance, nano-CoO was more toxic to *E. coli* than nano-Co$_3$O$_4$ (Table S5, SI). Toxicity of nano-TiO$_2$ to *E.coli* with the logarithm of EC$_{50}$ has been determined to be −1.60 (Dasari

et al., 2013), which is consistent with the predicted value −1.95. Due to the log–log scale, the predicted and the observed toxic endpoints for well-predicted MeONPs differ by a factor of two. This uncertainty could prevent their use in robust assessments of risk in regulatory decision-making. Therefore, an intelligent testing strategy that combines *in vivo* experiments with *in vitro* models and computational *in silico* methods, is needed to facilitate the risk analysis of MeONPs, and to support their risk management and regulatory oversight. In the context of paucity of robust experimental data for the multitude of existing and emerging nanoformulations, the proposed modeling approach can be an alternative solution to obtain predicted endpoint values in rapid, inexpensive, and reasonably accurate manner. The model has proved to be able to predict the toxicity of the MeONPs, and therefore can provide useful guidance for their regulation and safer design.

There are some fundamental differences in bioavailability and uptake. The chemistry and behavior of MeONPs involves dynamic aspects of aggregation theory, rather than the

equilibrium models traditionally used for free metal ions. Some MeONPs can release free metal ions from the surface of the particles. Biological uptake of nanomaterials is not only via endocytosis but also ion transporters, as well as Trojan-horse mechanisms (Hsiao et al., 2015). Optimal structural parameters can characterize energy of the lattice, reflecting dissolution and ionization potential of nanoparticles which is a good parameter to describe chemical stability. This process is related to the dissolution and redox reactions, which can release metal ions or produce free radicals that caused adverse effects on host bacteria. It was reported that mechanisms of toxicities of nanoscale metals and dissolved metals to fish vary among materials (Shaw & Handy, 2011). Composite mechanisms of oxidative stress and free metal ions, have been studied during experiments to measure ROS, concentrations of metal ions, reduced glutathione and lipid peroxidation (Neal, 2008).

Conclusions

A nano-QSAR model was developed to predict the cytotoxicity of 51 MeONPs to *E. coli* for which no empirical data were available. Based on the results of a previous study, the model was improved by use of additional structure parameter Z/r, which increased accuracy of prediction. The results of applying the two-variable model provide an evidence for understanding the key steps of the MeONPs, as well as released metal ions, to cause toxic potency in *E. coli*. The results of the study suggest that nano-QSARs can be a useful complementary method for hazard screening of MeONPs and their prioritization for further testing and risk assessment. In addition, it can provide excellent information supporting the safer design of nanomaterials.

Declaration of interest

References

Alaraby M, Hernandez A, Marcos R. 2016. New insights in the acute toxic/genotoxic effects of CuO nanoparticles in the in vivo Drosophila model. Nanotoxicology 26:1–12.

Base CF, Mesmer RE. 1976. The Hydrolysis of Cations. New York, USA: John Wiley and Sons Inc.

Brown D, Wilson M, MacNee W, Stone V, Donaldson K. 2001. Size-dependent proinflammatory effects of ultrafine polystyrene particles: a role for surface area and oxidative stress in the enhanced activity of ultrafines. Toxicol Appl Pharmacol 175:191–9.

Chen C, Mu YS, Wu FC, Zhang R, Su H, Giesy JP. 2015. Derivation of marine water quality criteria for metals based on a novel QICAR-SSD model. Environ Sci Pollut Res Int 22:4297–304.

Clark RD, Fox PC. 2004. Statistical variation in progressive scrambling. J Comput Aided Mol Des 18:563–76.

Dasari TP, Pathakoti K, Hwang HM. 2013. Determination of the mechanism of photoinduced toxicity of selected metal oxide nanoparticles (ZnO, CuO, Co_3O_4 and TiO_2) to *E. coli* bacteria. J Environ Sci 25:882–8.

De M, Ghosh PS, Rotello VM. 2008. Applications of nanoparticles in biology. Adv Mater 20:4225–41.

Dearden JC, Cronin MT, Kaiser KL. 2009. How not to develop a quantitative structure-activity or structure-property relationship (QSAR/QSPR). SAR QSAR Environ Res 20:241–66.

Epa VC, Burden FR, Tassa C, Weissleder R, Shaw S, Winkler DA. 2012. Modeling biological activities of nanoparticles. Nano Lett 12:5808–12.

Erdemir A, Li S, Jin Y. 2005. Relation of certain quantum chemical parameters to lubrication behavior of solid oxides. Int J Mol Sci 6: 203–18.

Eriksson L, Jaworska J, Worth AP, Cronin MT, McDowell RM, Gramatica P. 2003. Methods for reliability and uncertainty assessment and for applicability evaluations of classification- and regression-based QSARs . Environ Health Perspect 111:1361.

Gajewicz A, Puzyn T, Rasulev B, Leszczynska D, Leszczynski J. 2011. Metal oxide nanoparticles: size-dependence of quantum-mechanical properties. Nanosci Nanotechnol Asia 1:53–8.

Gliga AR, Skoglund S, Wallinder IO, Fadeel B, Karlsson HL. 2014. Size-dependent cytotoxicity of silver nanoparticles in human lung cells: the role of cellular uptake, agglomeration and Ag release. Part Fibre Toxicol 11:11.

Golbraikh A, Shen M, Xiao Z, Xiao YD, Lee KH, Tropsha A. 2003. Rational selection of training and test sets for the development of validated QSAR models. J Comput Aided Mol Des 17:241–53.

Heinlaan M, Ivask A, Blinova I, Dubourguier HC, Kahru A. 2008. Toxicity of nanosized and bulk ZnO, CuO and TiO_2 to bacteria Vibrio fischeri and crustaceans *Daphnia magna* and *Thamnocephalus platyurus.* Chemosphere 71:1308–16.

Hsiao IL, Hsieh YK, Wang CF, Chen IC, Huang YJ. 2015. Trojan-horse mechanism in the cellular uptake of silver nanoparticles verified by direct intra- and extracellular silver speciation analysis. Environ Sci Technol 49:3813–21.

Hu X, Cook S, Wang P, Hwang HM. 2009. In vitro evaluation of cytotoxicity of engineered metal oxide nanoparticles. Sci Total Environ 407:3070–2.

Kaiser KLE. 1980. Correlation and prediction of metal toxicity to aquatic biota. Can J Fish Aquat Sci 37:211–18.

Karlsson HL, Cronholm P, Gustafsson J, Moller L. 2008. Copper oxide nanoparticles are highly toxic: a comparison between metal oxide nanoparticles and carbon nanotubes. Chem Res Toxicol 21:1726–32.

Kubinyi H. 1993. QSAR: Hansch analysis and related approaches. Vieweg Adv Stud Comput Sci 7:115–37.

Lubick N. 2008. Nanosilver toxicity: ions, nanoparticles-or both? Environ Sci Technol 42:8617.

Lubick N. 2008. Risks of nanotechnology remain uncertain. Environ Sci Technol 42:1821–4.

Markets R. 2015. The Global Market for Metal and Metal Oxide Nanoparticles to 2025. Dublin, Ireland: Future Markets, Inc.

Mccloskey JT, Newman MC, Clark SB. 1996. Predicting the relative toxicity of metal ions using ion characteristics: Microtox® biolumin-escence assay. Environ Toxicol Chem 15:1730–7.

Meng H, Xia T, George S, Nel AE. 2009. A predictive toxicological paradigm for the safety assessment of nanomaterials. ACS Nano 3: 1620–7.

Mu YS, Wu FC, Chen C, Liu Y, Zhao X, Haiqing L, et al 2014. Predicting criteria continuous concentrations of 34 metals or metalloids by use of quantitative ion character-activity relationships-species sensitivity distributions (QICAR-SSD) model. Environ Pollut 188:50–5.

Neal A. 2008. What can be inferred from bacterium-nanoparticle interactions about the potential consequences of environmental exposure to nanoparticles? Ecotoxicology 17:362–71.

Negi H, Rathinavelu Saravanan P, Agarwal T, Ghulam Haider Zaidi M, Goel R. 2013. In vitro assessment of Ag_2O nanoparticles toxicity against Gram-positive and Gram-negative bacteria. J Gen Appl Microbiol 59:83–8.

Nel AE, Parak WJ, Chan WC, Xia T, Hersam MC, Brinker CJ, et al 2015. Where are we heading in nanotechnology environmental health and safety and materials characterization? ACS Nano 9:5627–30.

Pang CF, Brunelli A, Zhu CH, Hristozov D, Liu Y, Semenzin E, et al 2016. Demonstrating approaches to chemically modify the surface of Ag nanoparticles in order to influence their cytotoxicity and biodistribution after single dose acute intravenous administration. Nanotoxicology 10:129–39.

Pathakoti K, Huang MJ, Watts JD, He X, Hwang HM. 2014. Using experimental data of Escherichia coli to develop a QSAR model for predicting the photo-induced cytotoxicity of metal oxide nanoparticles. J Photoch Photobio B 130:234–40.

Pearson RG, Mawby RJ. 1967. The nature of metal-halogen bonds. Phys Rev D 66:55–84.

Puzyn T, Rasulev B, Gajewicz A, Hu X, Dasari TP, Michalkova A, et al 2011. Using nano-QSAR to predict the cytotoxicity of metal oxide nanoparticles. Nat Nanotechnol 6:175–8.

Sarkar A, Ghosh M, Sil PC. 2014. Nanotoxicity: oxidative stress mediated toxicity of metal and metal oxide nanoparticles. J Nanosci Nanotechnol 14:730–43.

Schrurs F, Lison D. 2012. Focusing the research efforts. Nat Nanotechnol 7:546–8.

Shaw BJ, Handy RD. 2011. Physiological effects of nanoparticles on fish: a comparison of nanometals versus metal ions. Environ Int 37:1083–97.

Tamura T. 2010. Introduction of MOPAC simulation for experimental biochemists. Seikagaku 82:863–7.

Topliss JG, Costello RJ. 1972. Change correlations in structure-activity studies using multiple regression analysis. J Med Chem 15:1066–8.

Tropsha A, Gramatica P, Gombar VK. 2003. The importance of being earnest: validation is the absolute essential for successful application and interpretation of QSPR models. QSAR Comb Sci 22:69–77.

Wang B, Zhang Y, Mao Z, Yu D, Gao C. 2014. Toxicity of ZnO nanoparticles to macrophages due to cell uptake and intracellular release of zinc ions. J Nanosci Nanotechnol 14:5688–96.

Wang D, Lin Z, Wang T, Yao Z, Qin M, Zheng S, et al 2016. Where does the toxicity of metal oxide nanoparticles come from: the nanoparticles, the ions, or a combination of both? J Hazard Mater 308:328–34.

Wilson MR, Lightbody JH, Donaldson K, Sales J, Stone V. 2002. Interactions between ultrafine particles and transition metals in vivo and in vitro. Toxicol Appl Pharmacol 184:172–9.

Winkler DA, Mombelli E, Pietroiusti A, Tran L, Worth A, Fadeel B, et al 2013. Applying quantitative structure-activity relationship approaches to nanotoxicology: current status and future potential. Toxicology 313: 15–23.

Wolterbeek HT, Verburg TG. 2001. Predicting metal toxicity revisited: general properties vs. specific effects. Sci Total Environ 279:87–115.

Wu FC, Meng W, Zhao X, Li H, Zhang R, Cao Y, et al 2010. China embarking on development of its own national water quality criteria system. Environ Sci Technol 44:7992–3.

Wu FC, Mu YS, Chang H, Zhao X, Giesy JP, Wu KB. 2013. Predicting water quality criteria for protecting aquatic life from physicochemical properties of metals or metalloids. Environ Sci Technol 47:446–53.

Yin N, Liu Q, Liu J, He B, Cui L, Li Z, et al 2013. Silver nanoparticle exposure attenuates the viability of rat cerebellum granule cells through apoptosis coupled to oxidative stress. Small 9:1831–41.

Zhai HJ, Wang LS. 2007. Probing the electronic structure and band gap evolution of titanium oxide clusters $(TiO(2))(n)(-)$ (n = 1–10) using photoelectron spectroscopy. J Am Chem Soc 129:3022–6.

Zhang H, Ji Z, Xia T, Meng H, Low-Kam C, Liu R, et al 2012. Use of metal oxide nanoparticle band gap to develop a predictive paradigm for oxidative stress and acute pulmonary inflammation. ACS Nano 6: 4349–68.

Zhao Q, Yang K, Li W, Xing B. 2014. Concentration-dependent polyparameter linear free energy relationships to predict organic compound sorption on carbon nanotubes. Sci Rep 4:1465–76.

Supplementary material available online

The Authors: Yunsong Mu, Fengchang Wu, Qing Zhao, Rong Ji, Yu Qie, Yue Zhou, Yan Hu, Chengfang Pang, Danail Hristozov, John P. Giesy, and Baoshan Xing

Manuscript entitled "Predicting Toxic Potencies of Metal Oxide Nanoparticles by Means of Nano-QSARs"

Number SI pages: 9

Number the tables: 5

Number the figures: 3

Table S1. The list of MeONPs and their structural properties

MeO NPs	ΔH_{me+}	σp	$\sigma p/Z$	AN	r	ΔIP	ΔE_0	X_m	|logK$_{OH}$|	$X_m^2 r$	Z^2/r	AN/ΔIP	AR	IP	IP(N+1)	AW	AR/AW	Z	Z/r^2	Z/AR^2	Z/r	Z/AR	x	z/rx	GAP	HoF
	kcal/mol	/	/	/	Å	eV	V	Å	/	/	/	/	Å	eV	eV	/	/	/	/	/	/	/	Å	/	eV	kcal/mol
ZnO	662.44	0.12	0.06	30	0.74	21.76	0.76	1.65	8.2	2.01	5.41	1.38	1.53	17.96	39.72	65.4	0.02	2	3.65	0.85	3	1.31	1.65	1.64	3.87	-5307
CuO	706.25	0.1	0.05	29	0.73	16.55	0.16	1.9	8	2.64	5.48	1.75	1.57	20.29	36.84	63.6	0.02	2	3.75	0.81	3	1.27	1.9	1.44	-3.85	-954.75
Y$_2$O$_3$	837.15	0.15	0.05	39	0.9	40.08	2.37	1.22	7.7	1.34	10	0.97	1.78	20.52	60.6	88.9	0.02	3	3.7	0.95	3	1.69	1.22	2.73	-2.48	-11486
Bi$_2$O$_3$	1137.4	0.11	0.04	83	1.03	19.74	0.2	2.02	1.09	4.2	8.74	4.2	1.46	25.56	45.3	209	0.01	3	2.83	1.41	3	2.05	2.02	1.44	-2.71	-1966
In$_2$O$_3$	1271.13	0.1	0.03	49	0.8	25.97	0.49	1.78	4	2.53	11.25	1.89	1.62	28.03	54	115	0.01	3	4.69	1.14	4	1.85	1.78	2.11	-4.79	-3088
Al$_2$O$_3$	1187.83	0.14	0.05	13	0.54	91.54	1.66	1.61	4.3	1.4	16.67	0.14	1.82	28.45	119.99	27	0.07	3	10.29	0.91	6	1.65	1.61	3.45	-4.59	-8244
Fe$_2$O$_3$	1408.29	0.1	0.03	26	0.55	24.15	0.77	1.83	2.2	1.84	16.36	1.08	1.72	30.65	54.8	55.9	0.03	3	9.92	1.01	5	1.74	1.83	2.98	-6.45	-1051
SnO$_2$	1717.32	0.08	0.02	50	0.69	31.54	0.15	1.96	3.4	2.65	23.19	1.59	1.4	40.74	72.28	119	0.01	4	8.4	2.04	6	2.86	1.96	2.96	-3.85	-2611
TiO$_2$	1575.73	0.1	0.03	22	0.61	56.03	0.5	1.54	2.2	1.45	26.23	0.39	1.45	43.27	99.3	47.9	0.03	4	10.75	1.9	7	2.76	1.54	4.26	-7.47	-9826
V$_2$O$_3$	1097.93	0.12	0.04	23	0.64	17.4	1	1.63	2.26	1.7	14.06	1.32	1.31	29.31	46.71	50.9	0.03	3	7.32	1.75	5	2.29	1.63	2.88	-4.17	-3192
Sb$_2$O$_3$	1233.06	0.12	0.04	51	0.76	18.9	0.66	2.05	2.72	3.19	11.84	2.7	1.53	25.3	44.2	113	0.01	3	5.19	1.28	4	1.96	2.05	1.93	-7.27	-2140
ZrO$_2$	1357.66	0.12	0.03	40	0.72	46.01	1.45	1.33	0.3	1.27	22.22	0.87	1.59	34.34	80.35	91.2	0.02	4	7.72	1.58	6	2.52	1.33	4.18	-1.65	-9834
CoO	601.8	0.13	0.07	27	0.65	16.42	0.28	1.88	9.7	2.3	6.15	1.64	1.67	17.08	33.5	58.9	0.03	2	4.73	0.72	3	1.2	1.88	1.64	-2.2	-8799
NiO	596.7	0.13	0.06	28	0.69	17.02	0.23	1.91	9.9	2.52	5.8	1.65	1.62	18.17	35.19	58.7	0.03	2	4.2	0.76	3	1.23	1.92	1.51	-4.73	63.89
Cr$_2$O$_3$	1268.7	0.11	0.04	24	0.62	18.2	0.41	1.66	4	1.71	14.52	1.32	1.85	30.96	49.16	52	0.04	3	7.8	0.88	5	1.62	1.66	2.91	-6.41	-2829
La$_2$O$_3$	1017.22	0.17	0.06	57	1.03	30.77	2.37	1.1	8.5	1.25	8.74	1.85	2.74	19.18	49.95	139	0.02	3	2.83	0.4	3	1.09	1.11	2.62		

2   Table S2. Pearson correlation coefficients (r) between structure properties of 26 MeONPs

	ΔH_{me+}	σp	$\sigma p/Z$	AN	r	ΔIP	ΔE_0	X_m	$|logK_{OH}|$	$X_m{}^2r$	Z^2/r	AN/ΔIP	AR	IP	IP(N+1)	AW	AR/AW	Z	Z/r^2	Z/AR^2	Z/r	Z/AR	x	z/rx	GAP	HoF
ΔH_{me+}	1.000	-.607	-.974	.175	-.209	.349	-.018	-.037	-.839	-.097	.896	-.135	-.204	.945	.591	.186	-.074	.912	.718	.759	.856	.855	-.041	.699	-.510	-.021
σp		1.000	.649	-.212	.151	.253	.656	-.455	.367	-.278	-.405	-.147	.412	-.590	.021	-.215	.341	-.361	-.294	-.489	-.361	-.461	-.452	-.084	.239	-.509
$\sigma p/Z$			1.000	-.272	.066	-.245	.024	.075	.854	.053	-.848	.057	.281	-.925	-.498	-.284	.221	-.911	-.599	-.794	-.773	-.877	.080	-.651	.438	-.016
AN				1.000	.852	-.325	-.230	.378	-.333	.784	-.114	.854	-.351	.006	-.267	.998	-.777	.197	-.506	.292	-.302	.273	.376	-.355	.113	.245
r					1.000	-.316	.026	.075	-.008	.605	-.393	.736	-.211	-.313	-.362	.850	-.705	-.062	-.769	.031	-.588	.000	.074	-.467	.335	.033
ΔIP						1.000	.569	-.494	-.244	-.515	.545	-.609	.287	.401	.956	-.298	.652	.454	.600	.162	.582	.288	-.494	.672	-.104	-.609
ΔE_0							1.000	-.812	-.078	-.632	.159	-.495	.384	-.044	.457	-.228	.310	.223	.149	-.069	.176	.044	-.812	.459	.174	-.666
X_m								1.000	.069	.831	-.320	.667	-.293	-.158	-.459	.366	-.252	-.325	-.241	-.057	-.297	-.167	1.000	-.639	-.229	.775
$|logK_{OH}|$									1.000	-.026	-.711	-.105	.303	-.758	-.444	-.349	.159	-.805	-.522	-.711	-.666	-.780	.074	-.592	.374	-.011
$X_m{}^2r$										1.000	-.419	.945	-.371	-.245	-.504	.778	-.562	-.241	-.568	.018	-.509	-.082	.831	-.715	-.017	.618
Z^2/r											1.000	-.457	-.176	.961	.758	-.100	.115	.934	.847	.766	.964	.868	-.322	.911	-.415	-.324
AN/ΔIP												1.000	-.343	-.294	-.598	.848	-.665	-.216	-.657	.012	-.564	-.076	.666	-.688	.062	.533
AR													1.000	-.288	.145	-.354	.549	-.231	.079	-.725	-.048	-.554	-.292	.059	-.105	-.231
IP														1.000	.652	.024	.000	.918	.784	.821	.913	.896	-.161	.800	-.470	-.132
IP(N+1)															1.000	-.239	.540	.669	.747	.396	.774	.525	-.461	.812	-.237	-.546
AW																1.000	-.752	.209	-.487	.305	-.286	.286	.364	-.338	.120	.232
AR/AW																	1.000	-.138	.545	-.365	.322	-.295	-.251	.332	-.173	-.247
Z																		1.000	.636	.830	.834	.936	-.328	.818	-.360	-.319
Z/r^2																			1.000	.435	.954	.531	-.242	.845	-.499	-.215
Z/AR^2																				1.000	.636	.973	-.060	.551	-.218	-.093
Z/r																					1.000	.742	-.299	.916	-.489	-.273
Z/AR																						1.000	-.170	.682	-.284	-.190
x																							1.000	-.641	-.229	.777
z/rx																								1.000	-.306	-.549
GAP																									1.000	-.246
HoF																										1.000

3   Table S3. Internal validation of QSAR model

	Bootstrapping	Leave-one-out	Leave-many-out n=3	Progressive scrambling analysis		
				Q^2	SEP_{CV}	dq^2/dr^2_{yy}
R^2	0.910	0.855	0.846	0.579	0.366	1.109
Standard error	0.153	0.217	0.223			

4   Table S4. Predicted cytotoxicity (log $1/EC_{50}$) of 51 MeONPs obtained by multiple linear regression

ID	MeONPs	ΔH_{me+}	Z/r	Obs. log $1/EC_{50}$	Pred. log $1/EC_{50}$	Residuals
1	ZnO	662.44	2.703	3.45	3.39	0.06
2	CuO	713.74	2.740	3.20	3.35	-0.15
3	Y_2O_3	837.15	3.333	2.87	3.13	-0.26
4	Bi_2O_3	1137.40	2.913	2.82	2.87	-0.05
5	In_2O_3	1271.13	3.750	2.81	2.62	0.19
6	Al_2O_3	1187.83	5.556	2.49	2.46	0.03
7	Fe_2O_3	1363.40	5.455	2.29	2.25	0.04
8	SnO_2	1717.32	5.797	2.01	1.89	0.12
9	TiO_2	1575.73	6.557	1.74	1.95	-0.21
10	V_2O_3	1097.73	4.688	3.14	2.69	0.45
11	Sb_2O_3	1233.06	3.947	2.64	2.62	0.02
12	ZrO_2	1357.66	5.556	2.15	2.31	-0.16
13	CoO	594.59	3.077	3.51	3.39	0.12
14	NiO	596.88	2.899	3.45	3.42	0.03
15	Cr_2O_3	1266.62	4.839	2.51	2.48	0.03
16	La_2O_3	1017.22	2.913	2.87	3.04	-0.17
Prediction set						
17	BeO	657.34	4.444	N/A	3.22	N/A
18	MgO	543.10	2.778	N/A	3.53	N/A
19	CaO	407.29	2.020	N/A	3.76	N/A
20	SrO	413.87	1.786	N/A	3.78	N/A
21	BaO	388.71	1.481	N/A	3.84	N/A
22	Sc_2O_3	874.35	4.000	N/A	3.05	N/A
23	HfO_2	1555.34	4.819	N/A	2.27	N/A
24	Nb_2O_3	1312.47	4.167	N/A	2.60	N/A
25	Ta_2O_3	1368.16	4.167	N/A	2.54	N/A
26	Mo_2O_3	1306.84	4.348	N/A	2.58	N/A

27	WO_2	2005.58	6.061	N/A	1.67	N/A
28	MnO_2	1602.05	7.547	N/A	1.90	N/A
29	TcO_2	2114.98	6.154	N/A	1.55	N/A
30	ReO_2	1780.23	6.349	N/A	1.86	N/A
31	RuO_2	1674.84	6.452	N/A	1.96	N/A
32	OsO_2	1757.52	6.349	N/A	1.89	N/A
33	Rh_2O_3	960.20	4.478	N/A	2.91	N/A
34	IrO_2	1410.10	6.349	N/A	2.23	N/A
35	PdO	657.34	4.444	N/A	3.22	N/A
36	PtO_2	2165.13	6.349	N/A	1.48	N/A
37	Ag_2O	233.51	0.870	N/A	4.07	N/A
38	Au_2O_3	1289.31	3.529	N/A	2.70	N/A
39	CdO	548.22	2.105	N/A	3.61	N/A
40	HgO	679.86	1.961	N/A	3.49	N/A
41	Ga_2O_3	1384.15	4.839	N/A	2.44	N/A
42	Tl_2O	207.75	0.629	N/A	4.13	N/A
43	GeO_2	1857.61	7.547	N/A	1.64	N/A
44	PbO	499.19	1.681	N/A	3.71	N/A
45	PbO_2	1994.02	5.128	N/A	1.80	N/A
46	Co_3O_4	811.12	4.603	3.00	2.94	0.06
47	PtO	813.94	2.500	N/A	3.30	N/A
48	Au_2O	314.86	0.730	N/A	4.01	N/A
49	Tl_2O_3	1341.37	3.371	N/A	2.66	N/A
50	Mn_2O_3	1017.99	5.172	3.08	2.77	0.36
51	Co_2O_3	919.39	5.505	N/A	2.83	N/A

5   Table S5. Predicted cytotoxicity of MeONPs with various valences of metals

| Compounds	ΔH_{me+}	Z/r	Pred. log $1/EC_{50}$
CoO	594.59	3.077	3.39
Co_3O_4	811.12	4.603	2.94
Co_2O_3	919.39	5.505	2.83
PbO	499.19	1.681	3.71
PbO_2	1994.02	5.128	1.80
PtO	813.94	2.500	3.30
PtO_2	2165.13	6.349	1.48
Au_2O	314.86	0.730	4.01
Au_2O_3	1289.31	3.529	2.70
Tl_2O	207.75	0.629	4.13
Tl_2O_3	1341.37	3.371	2.66
Mn_2O_3	1017.99	5.172	2.77
MnO_2	1602.05	7.547	1.9
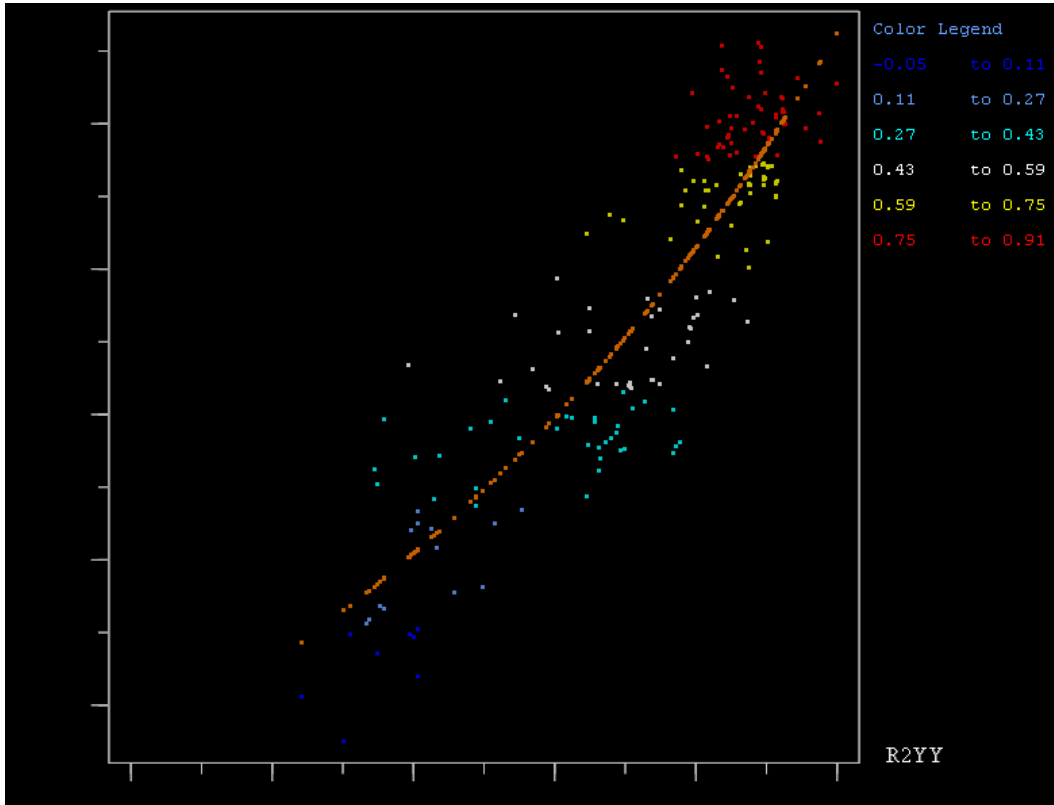
6

7   Figure S1. Results of progressive scrambling plot: q^2/fitted q^2 versus r^2yy
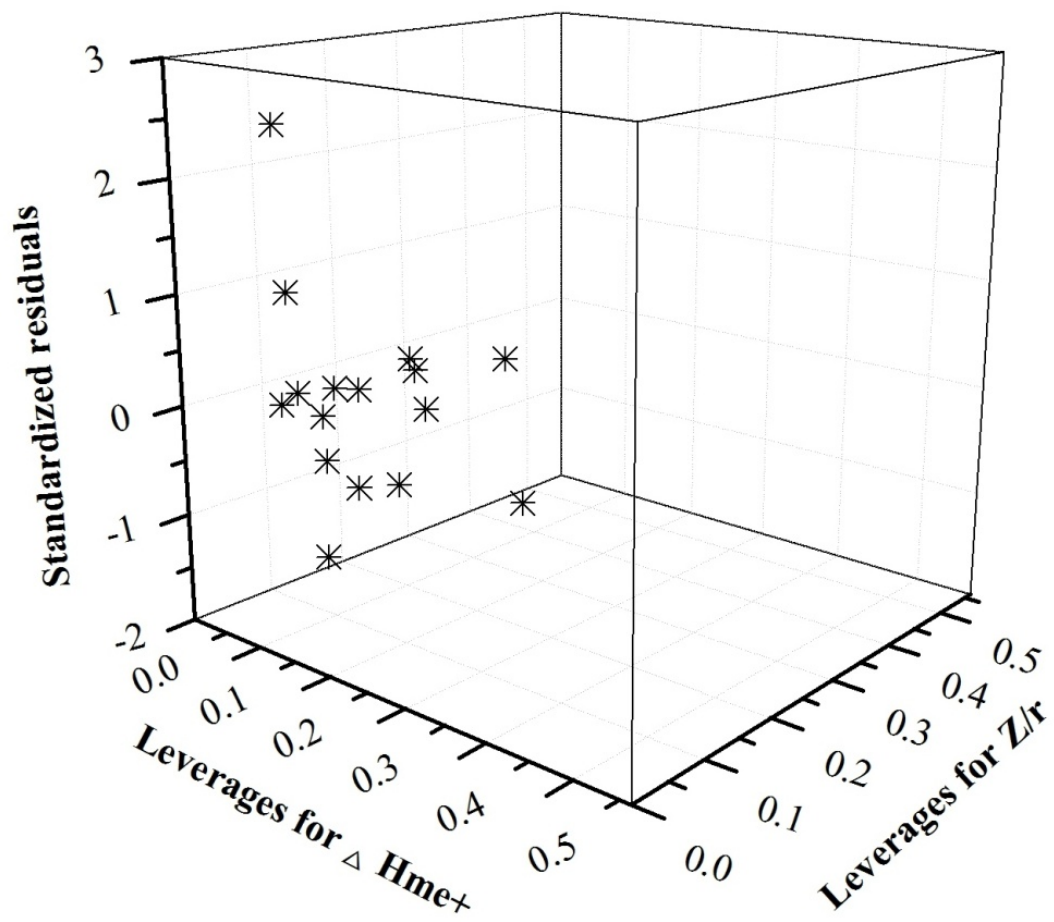
8

9   Figure S2. The Williams plot
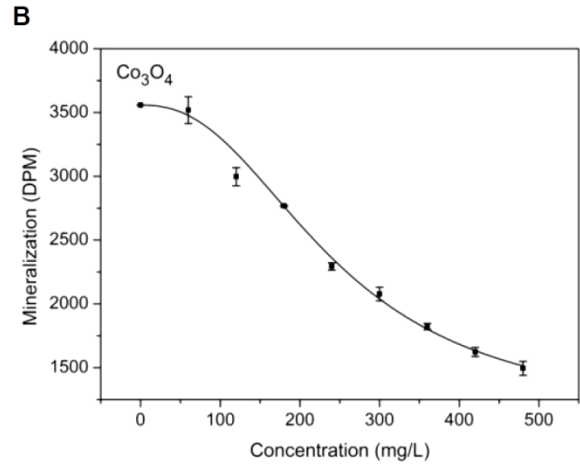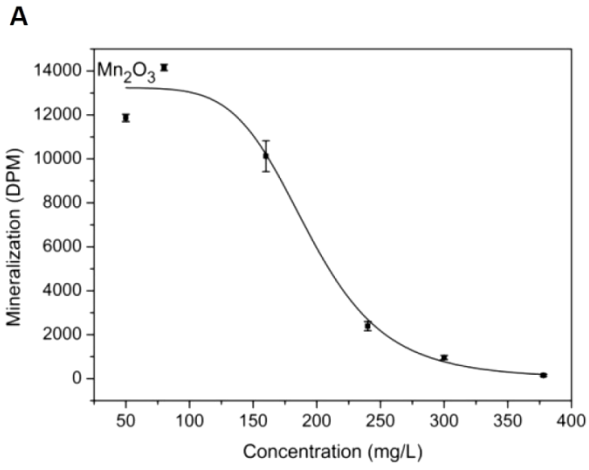
10

11   Figure S3. Dose–response curve of nano Mn_2O_3 (a) and Co_3O_4 (b) used for external validation